arXiv:1609.05506v1 [nucl-ex] 18 Sep 2016

version 1, September 20, 2016

Experimental results on chiral magnetic and vortical effects

Gang Wang[1] and Liwen Wen[1]

[1]*Department of Physics and Astronomy, University of California, Los Angeles, California 90095, USA*

Various novel transport phenomena in chiral systems result from the interplay of quantum anomalies with magnetic field and vorticity in high-energy heavy-ion collisions, and could survive the expansion of the fireball and be detected in experiments. Among them are the chiral magnetic effect, the chiral vortical effect and the chiral magnetic wave, the experimental searches for which have aroused extensive interest. The goal of this review is to describe the current status of experimental studies at Relativistic Heavy Ion Collider at BNL and the Large Hadron Collider at CERN, and to outline the future work in experiment needed to eliminate the existing uncertainties in the interpretation of the data.

PACS numbers: 25.75.Ld

I. INTRODUCTION

High-energy heavy-ion collisions can produce a hot, dense, and deconfined nuclear medium, dubbed the quark-gluon plasma (QGP). The thermodynamic states of a QGP can be specified by the axial chemical potential μ_5, besides the temperature T and the vector chemical potential μ. μ_5 characterizes the imbalance of right-handed and left-handed fermions in a system, and a *chiral* system bears a nonzero μ_5. Chiral domains may be created locally in heavy-ion collisions through various mechanisms on an event-by-event basis (e.g. topological fluctuations in the gluonic sector, glasma flux tubes, or fluctuations in the quark sector) [1–6]. In a noncentral collision, a strong magnetic field ($B \sim 10^{15}$ T) can be produced (mostly by energetic spectator protons) [2, 3], and will induce an electric current along $\overrightarrow{B}$ in chiral domains, $\overrightarrow{J_e} \propto \mu_5 \overrightarrow{B}$, which is called the chiral magnetic effect (CME) [1, 2]. On average, $\overrightarrow{B}$ is perpendicular to the so-called reaction plane ($\Psi_{\rm RP}$) that contains the impact parameter and the beam momenta, as depicted in Fig. 1. Hence the CME will manifest a charge transport across the reaction plane.

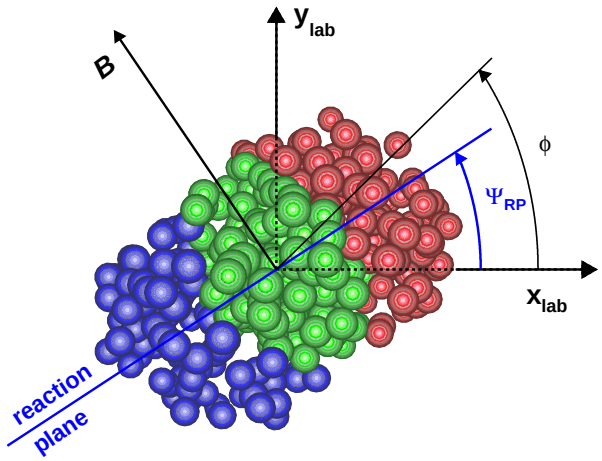

FIG. 1: Schematic depiction of the transverse plane for a collision of two heavy ions (the left one emerging from and the right one going into the page). Particles are produced in the overlap region (green-colored nucleons). The azimuthal angles of the reaction plane and a produced particle are depicted here.

In the presence of the CME and other modes of collective motions, we can Fourier decompose the azimuthal distribution of particles of given transverse momentum (p_T) and pseudorapidity (η):

$$\frac{dN_\alpha}{d\phi} \propto 1 + 2v_{1,\alpha}\cos(\Delta\phi) + 2v_{2,\alpha}\cos(2\Delta\phi) + ... + 2a_{1,\alpha}\sin(\Delta\phi) + ..., \quad (1)$$

where ϕ is the azimuthal angle of a particle, and $\Delta\phi = \phi - \Psi_{\rm RP}$. Here the subscript α (+ or −) denotes the charge sign of the particle. Conventionally v_1 is called "directed flow" and v_2 "elliptic flow" [7]. The parameter a_1 (with $a_{1,-} = -a_{1,+}$) quantifies the electric charge separation due to the CME.

An anomalous transport effect can also occur when a chiral system undergoes a global rotation. The fluid rotation can be quantified by a vorticity $\vec{\omega} = \vec{\nabla} \times \vec{v}$, where $\vec{v}$ is the flow velocity field. For a given vorticity $\vec{\omega}$, the chiral vortical effect (CVE) induces a vector current $\vec{J_{\rm v}} \propto \mu_5 \mu_{\rm v} \vec{\omega}$ [8]. While the CME is driven by $\vec{B}$, the CVE is driven by $\mu_{\rm v}\vec{\omega}$ in a chiral medium. Here the subscript "v" means "vector", and can be, for example, "B" (baryon) or "e" (electron). In heavy-ion collisions, μ_B is typically larger than μ_e by an order of magnitude, making it easier to search for the CVE via the baryonic charge separation than the electric charge separation. Hence the subscript α in Eq. 1 represents baryon or anti-baryon in the CVE search.

Another complementary transport phenomenon to the CME has been found and named the chiral separation effect (CSE) [9, 10], in which chiral charges are separated along the axis of the magnetic field in the presence of finite density of vector charge: $\vec{J_5} \propto \mu_{\rm v}\vec{B}$. In a chirally symmetric phase, the CME and CSE form a collective excitation, the chiral magnetic wave (CMW), a long wavelength hydrodynamic mode of chiral charge densities [11, 12]. The CMW, a signature of the chiral symmetry restoration, manifests itself in a finite electric quadrupole moment of the collision system, where the "poles" ("equator") of the produced fireball acquire additional positive (negative) charge [11]. This effect, if present, will be reflected in the measurements of charge-dependent elliptic flow.

There are other chiral magnetic/vortical effects such as the chiral electric separation effect (CESE) [13, 14] and the chiral vortical wave (CVW) [15]; see Ref [16] for a recent review on these effects. This article reviews the experimental results in the past decade to search for the chiral magnetic/vortical effects in high-energy heavy-ion collisions: evidence for the initial magnetic field and vorticity in Sec. II, the observation of the electric (baryonic) charge separation in Sec. III (Sec. IV), and the manifestation of the electric quadrupole moment in Sec. V. An outlook for future development is discussed in Sec. VI.

II. DRIVING FORCE

We may intuitively regard the magnetic field (vorticity) as the driving force of the CME (CVE), while the chirality imbalance is the initial condition, and the electric (baryonic) charge separation is the manifestation. A rough estimate of the initial magnetic field gives $eB \sim \gamma\alpha_{\rm EM}Z/b^2$, where $\alpha_{\rm EM} \simeq 1/137$, b is the impact parameter, and γ is the Lorentz factor. Therefore a typical Au+Au collision at $\sqrt{s_{\rm NN}} = 200$ GeV produces $eB \sim 1/(1{\rm fm}^2) \sim m_\pi^2$. Many computations have attempted to quantify the electromagnetic field on the event-by-event basis (see e.g. [17–19]), in terms of the spatial distribution, the orientation fluctuation as well as the dependence on colliding nuclei, centrality and beam energy.

A major uncertainty in theoretical calculations of the magnetic field $\vec{B}$ is its duration in the QCD fluid created in the heavy-ion collision (see e.g. [20–23]). The time dependence of $\vec{B}$ after the impact of the two nuclei crucially depends on whether/when/how a conducting medium may form and the lifetime of the magnetic field may be elongated. The electric conductivity [24] and the time evolution of the quark densities [25] can be studied via directed flow of charged hadrons in asymmetric collisions, such as Cu+Au. Figure 2 illustrates the transverse plane for a Cu+Au collision with $b = 6$ fm [26]. The difference in the number of protons creates a strong electric field in the initial stage of the collision, pointing along the arrow in the figure. The lifetime of the electric field might be very short (e.g. $t \sim 0.25$ fm/c from Ref. [24, 25]), but the electric charges from quarks and antiquarks that are present in the early stage of the collision would experience the Coulomb force and lift the degeneracy in v_1 between positively and negatively charged particles [18, 24]:

$$v_1^{\pm} = v_1 \pm d_E \left\langle \cos(\Psi_{\rm RP} - \Psi_E) \right\rangle , \tag{2}$$

where Ψ_E denotes the azimuthal angle of the electric field, and the coefficient d_E characterizes the strength of dipole deformation induced by the electric field and is proportional to the electric conductivity of the medium. Here v_1 represents the rapidity-even component of directed flow that is dominant in asymmetric collisions, while in symmetric collisions v_1 conventionally denotes the rapidity-odd component.

Figure 3 shows recent STAR measurements of charge-dependent $v_1^{\rm even}$ and the difference $\Delta v_1^{\rm even}$ as functions of p_T in $10-40\%$ Cu+Au and Au+Au collisions [26]. For $p_T < 2$ GeV/c, $\Delta v_1^{\rm even}$ seems to increase with p_T. The $v_1^{\rm even}$ results from Au+Au collisions have much smaller values, roughly by a factor of 10, than those in Cu+Au. Note that $v_1^{\rm odd}$ in Au+Au collisions is similarly small [27]. $\Delta v_1^{\rm even}$ in Au+Au is consistent with zero. Calculations for charged pions from the parton-hadron-string-dynamics (PHSD) model [25], which is a dynamical transport approach in the partonic and hadronic phases, are compared with the data. The PHSD model calculates two cases: charge-dependent $v_1^{\rm even}$ with and without the initial electric field (EF). In the case with the EF switched on, the model assumes that

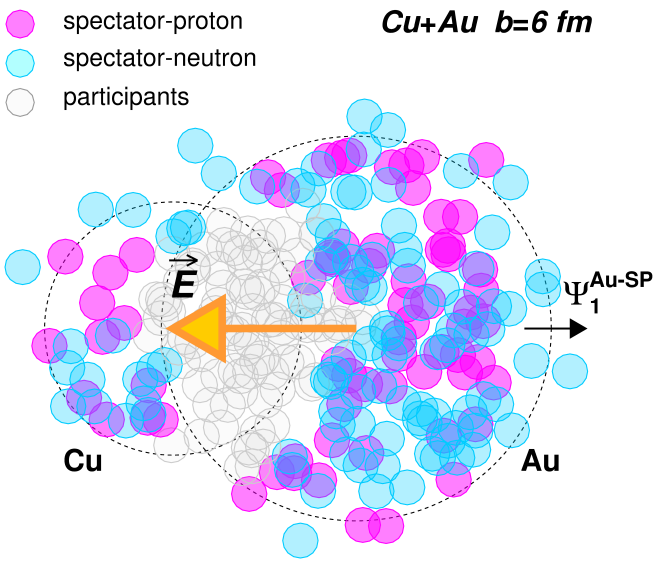

FIG. 2: Example of a noncentral Cu+Au collision viewed in the transverse plane showing an initial electric field $\vec{E}$ caused by the charge difference between the two nuclei [26]. $\Psi_1^{\mathrm{Au-SP}}$ denotes the direction of Au spectators.

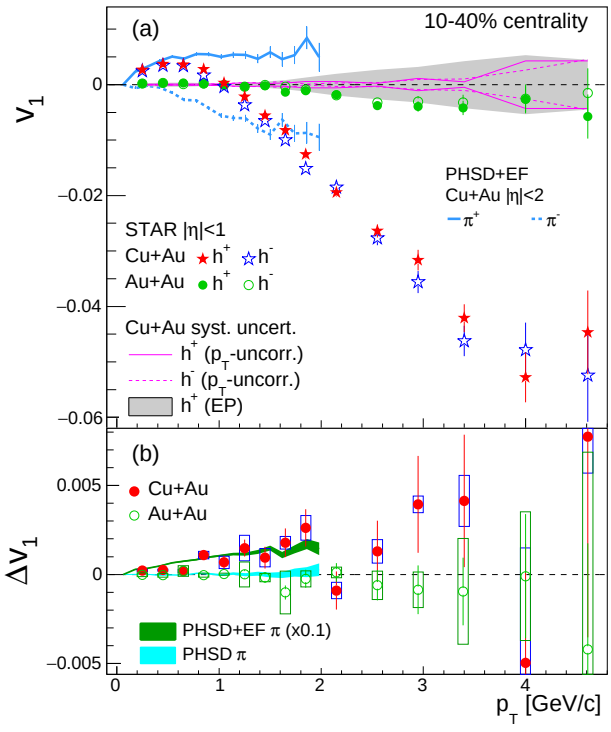

FIG. 3: v_1^{even} of positive and negative particles and the difference between the two as functions of p_T in $10-40\%$ Cu+Au and Au+Au collisions [26]. The PHSD model calculations [25] for charged pions with and without the initial electric field (EF) are presented for comparison.

all electric charges are affected by the EF and this results in a large separation of v_1^{even} between positive and negative particles as shown in Fig. 3(a). In Fig. 3(b), the calculations of the v_1^{even} with and without the EF are shown together, but note that the EF-on calculation points are scaled by 0.1. After scaling by 0.1, the model describes rather well the p_T dependence of the measured data for $p_T < 2$ GeV/c. This qualitative evidence for the strong initial electric field in asymmetric collisions provides an indirect evidence for the strong initial magnetic field in heavy-ion collisions that could leave an imprint on the final-stage particles.

The vorticity is induced by the global rotation of the QGP in heavy-ion collisions. In a noncentral collision, the majority of the global angular momentum, $\vec{L}$, is carried away by spectator nucleons. However, a considerable fraction (about $10-20\%$) of $\vec{L}$ could remain in the QGP and be approximately conserved in time [28, 29]. This implies a relatively long duration of the vortical effects. On average, the angular momentum is pointing in the out-of-plane direction, so the CME and CVE are very much alike in terms of their experimental observables. Attempts to computate local vorticity $\vec{\omega}$ and its space-time distribution have also been made [28–33].

Experimentally global polarization of hyperons such as Λ provides a measure for both the plasma vorticity and the magnetic field. Whereas the vortical effects will generate a positive polarization for both Λ and $\bar{\Lambda}$, the coupling of the hadronic magnetic dipole moment to the magnetic field will generate a positive contribution for Λ and a negative one for $\bar{\Lambda}$. Therefore, a splitting between Λ and $\bar{\Lambda}$ polarization will be a direct evidence for the strong initial magnetic field. Recently, preliminary STAR measurements [34] have reported the first observation of global Λ and $\bar{\Lambda}$ polarization in heavy-ion collisions. At $\sqrt{s_{\mathrm{NN}}} < 100$ GeV, the signal is on the order of a few percent, and displays a weak beam-energy dependence. The average polarization over Λ and $\bar{\Lambda}$ evidences the plasma vorticity, while the splitting observation requires much higher statistics to be delivered in the second beam energy scan (BES-II) program at RHIC [35] to signify the magnetic field.

The future search for evidence for the initial magnetic field (vorticity) is proposed via photon (vector meson) polarization measurements [36]. The initial magnetic helicity ($\vec{E} \cdot \vec{B}$) of the collision system can be quite large and bears opposite signs in the upper and lower hemispheres. Owing to the chiral anomaly, the helicity can be transferred back and forth between the magnetic flux and fermions as the collision system evolves, so that the magnetic helicity

could last long enough to yield photons with opposite circular polarizations in the hemispheres above and below the RP [37–39]. A similar asymmetry in photon polarization can also result from the initial global quark polarization [40], which could effectively lead to a polarization of photons [38]. This local imbalance of photon circular polarization could be observed in experiments, e.g., by studying the polarization preference with respect to the RP for photons that convert into e^+e^- pairs [36]. Similarly, vector mesons that decay into two daughters can also have their polarization preferences measured with the scheme outlined in Ref. [36], and the helicity separation in this case originates from vorticity [40–42].

III. CHIRAL MAGNETIC EFFECT

The discovery of the CME in high-energy heavy-ion collisions would confirm the simultaneous existence of ultra-strong magnetic fields, chiral symmetry restoration and topological charge changing transitions. The experimental searches for the CME have been carried out extensively in the past decade at RHIC and the LHC. This section will introduce the observables pertinent to the electric charge separation induced by the CME, present the experimental results and discuss the background contributions due to the coupling of elliptic flow and other physics mechanisms.

A. Charge-separation observable

From event to event, the signs of the μ_5 values are equally likely, and the signs of finite $a_{1,+}$ and $a_{1,-}$ will flip accordingly, leading to $\langle a_{1,+}\rangle = \langle a_{1,-}\rangle = 0$. Figure 4 presents the STAR measurements of $\langle a_{\pm}\rangle$ with the 1$^{\rm st}$ harmonic event plane reconstructed from spectator neutrons [43]. These results indicate no significant charge dependence in all centrality intervals, with the typical difference between positive and negative charges less than 10^{-4}.

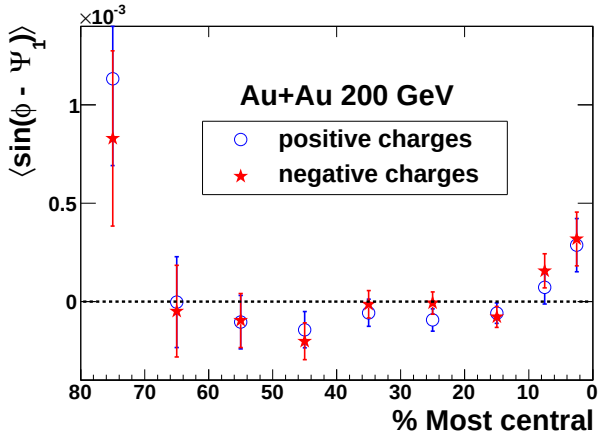

FIG. 4: $\langle \sin(\phi - \Psi_1)\rangle$ for positive and negative charges versus centrality for Au+Au collisions at $\sqrt{s_{\rm NN}} = 200$ GeV [43].

One therefore has to search for the CME with charge-separation *fluctuations* perpendicular to the reaction plane, e.g., with a three-point correlator [44], $\gamma \equiv \langle\langle \cos(\phi_\alpha + \phi_\beta - 2\Psi_{\rm RP})\rangle\rangle$, where the averaging is done over all particles in an event and over all events. In practice, the reaction plane is approximated with the "event plane" ($\Psi_{\rm EP}$) reconstructed with measured particles, and then the measurement is corrected for the finite event plane resolution. The expansion of the γ correlator,

$$\begin{aligned}\langle\langle \cos(\phi_\alpha + \phi_\beta - 2\Psi_{\rm RP})\rangle\rangle &= \langle\langle \cos(\Delta\phi_\alpha)\cos(\Delta\phi_\beta) - \sin(\Delta\phi_\alpha)\sin(\Delta\phi_\beta)\rangle\rangle \\ &= (\langle v_{1,\alpha} v_{1,\beta}\rangle + B_{\rm IN}) - (\langle a_{1,\alpha} a_{1,\beta}\rangle + B_{\rm OUT}), \end{aligned} \quad (3)$$

reveals the difference between the *in-plane* and *out-of-plane* projections of the correlations. The first term ($\langle v_{1,\alpha} v_{1,\beta}\rangle$) in the expansion provides a baseline unrelated to the magnetic field. The background contribution ($B_{\rm IN} - B_{\rm OUT}$) is suppressed to a level close to the magnitude of v_2 [44].

The STAR Collaboration first measured the γ correlator with the 2$^{\rm nd}$ harmonic event plane for Au+Au (shown with crosses in Fig. 5) and Cu+Cu (not shown here) collisions at 62.4 and 200 GeV with data from the 2004/2005 RHIC runs [45, 46]. All the results have been found to be in qualitative expectation with the CME: the opposite-charge ($\gamma_{\rm OS}$) and the same-charge ($\gamma_{\rm SS}$) correlations display the "right" ordering. The opposite-charge correlations in Cu+Cu

collisions are stronger than those in Au+Au, possibly reflecting the suppression of the correlations among oppositely moving particles in a larger system. STAR also presented p_T and $\Delta\eta$ dependences of the signal. The signal has a $\Delta\eta$ width of about one unit of rapidity, consistent with small chiral domains. The signal is found to increase with the pair average p_T, and it was later shown [47] that the radial flow expansion can explain this feature.

Similar γ results for 200 GeV Au+Au and 2.76 TeV Pb+Pb were observed by the PHENIX Collaboration [48] and the ALICE Collaboration [49], respectively. PHENIX also employed a multiparticle charge-sensitive correlator, $C_c(\Delta S)$ [50], and their preliminary results showed a concave $C_c(\Delta S)$ distribution, also evidencing the charge separation effect. The background from conventional physics was studied with heavy-ion event generators MEVSIM [51], UrQMD [52] and HIJING [53] (with and without an elliptic flow afterburner implemented). None of these generators could achieve reasonable agreement with the data. However, these generators do not provide particularly good descriptions of heavy-ion collisions, so the fact that they fail to describe such subtle effects as charge separation provides only somewhat limited support for a CME interpretation of the data.

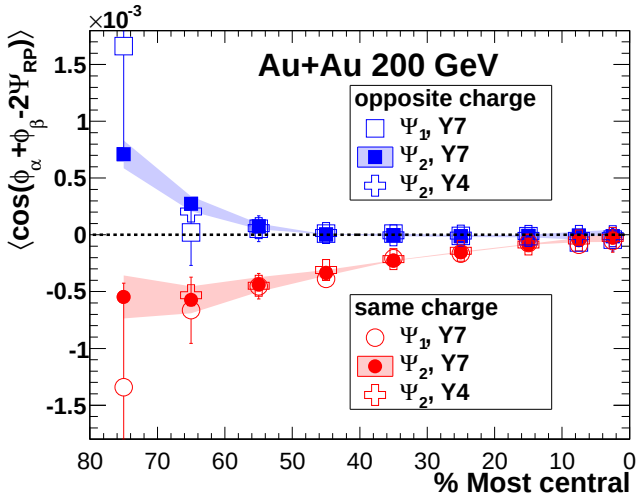

FIG. 5: Three-point correlator, γ, measured with 1st and 2nd harmonic event planes versus centrality for Au+Au collisions at $\sqrt{s_{\rm NN}}$ = 200 GeV [43]. Shown with crosses are STAR previous results from the 2004 RHIC run [45, 46].

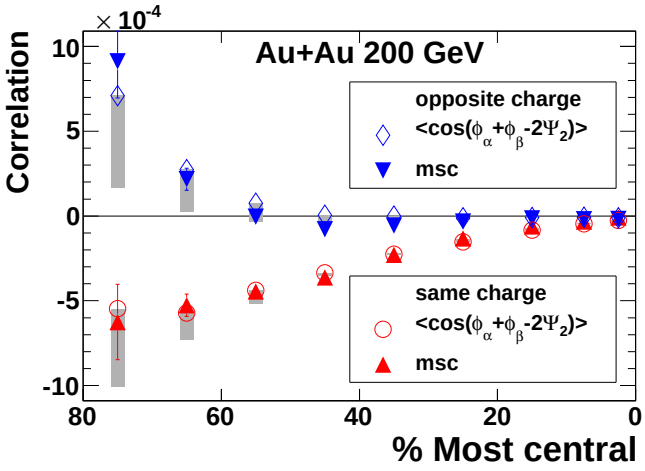

FIG. 6: Modulated sign correlations (msc) compared to the three-point correlator versus centrality for Au+Au collisions at $\sqrt{s_{\rm NN}}$ = 200 GeV [43]. The grey bars reflect the conditions of $\Delta p_T > 0.15$ GeV/c and $\Delta\eta > 0.15$ applied to γ.

The charge-separation signal was cross-checked with data from the 2007 RHIC run (shown in Fig. 5) [43]. The γ correlations from these data were measured with respect to both the 1st harmonic event plane (of spectators at large rapidity) and the 2nd harmonic event planes at mid-rapidity. Using the 1st harmonic event plane determined by spectator neutrons ensures that the signal is not coming from three-particle background correlations, and is due to genuine correlations to the reaction plane.

Another test was carried out by replacing one of the two charged particles in γ with a neutral particle, e.g. K^0_S, and the results show no separation between $K^0_S - h^+$ and $K^0_S - h^-$ [54]. Thus the charge separation observed in the γ correlation between two charged particles is indeed due to the electric charge. Femtoscopic correlations are visible in the differential measurements of γ at low relative momenta, which are related to quantum interference ("HBT") and final-state-interactions (Coulomb dominated) [43]. The difference between in-plane and out-of-plane correlations in the femtoscopic region can be due to a difference in the emission volumes probed by in- and out-of-plane parts. Such a difference may arrise from an azimuthally anisotropic freeze-out distribution coupled with flow. To suppress the contribution from femtoscopic correlations, the conditions of $\Delta p_T > 0.15$ GeV/c and $\Delta\eta > 0.15$ were applied to the three-point correlator, shown with the grey bars in Fig. 6. Excluding pairs with low relative momenta significantly reduces the positive contributions to opposite-charge correlations in peripheral collisions, but the difference between same- and opposite-charge correlations remains largely unchanged and consistent with the expectations of the CME.

The γ correlator weights different azimuthal regions of charge separation differently, i.e. oppositely charged pairs emitted azimuthally at 90° from the event plane (maximally out-of-plane) are weighted more heavily than those emitted only a few degrees from the event plane (minimally out-of-plane). It is a good test to modify the γ correlator such that all azimuthal regions of charge separation are weighted identically. This may be done by first rewriting Eq. 3 as

$$\langle \cos(\phi_\alpha + \phi_\beta - 2\Psi_{\rm RP}) \rangle = \langle (M_\alpha M_\beta S_\alpha S_\beta)_{\rm IN} \rangle - \langle (M_\alpha M_\beta S_\alpha S_\beta)_{\rm OUT} \rangle, \quad (4)$$

where M and S stand for the absolute magnitude ($0 \leq M \leq 1$) and the sign (± 1) of the sine or cosine function, respectively. IN represents the cosine part of Eq. 3 (in-plane) and OUT represents the sine part (out-of-plane). A modulated sign correlation (msc) is obtained by reducing the γ correlator [43]:

$$\text{msc} \equiv \left(\frac{\pi}{4}\right)^2 \left(\langle S_\alpha S_\beta \rangle_{\text{IN}} - \langle S_\alpha S_\beta \rangle_{\text{OUT}}\right). \tag{5}$$

The modulated sign correlations are compared with the three-point correlator for Au+Au collisions at 200 GeV in Fig. 6. It is evident that the msc is able to reproduce the same trend as the three-point correlator although their magnitudes differ slightly. STAR also carried out another approach called the charge multiplicity asymmetry correlation (CMAC), whose methodology is similar to the msc, and yielded very similar results [55].

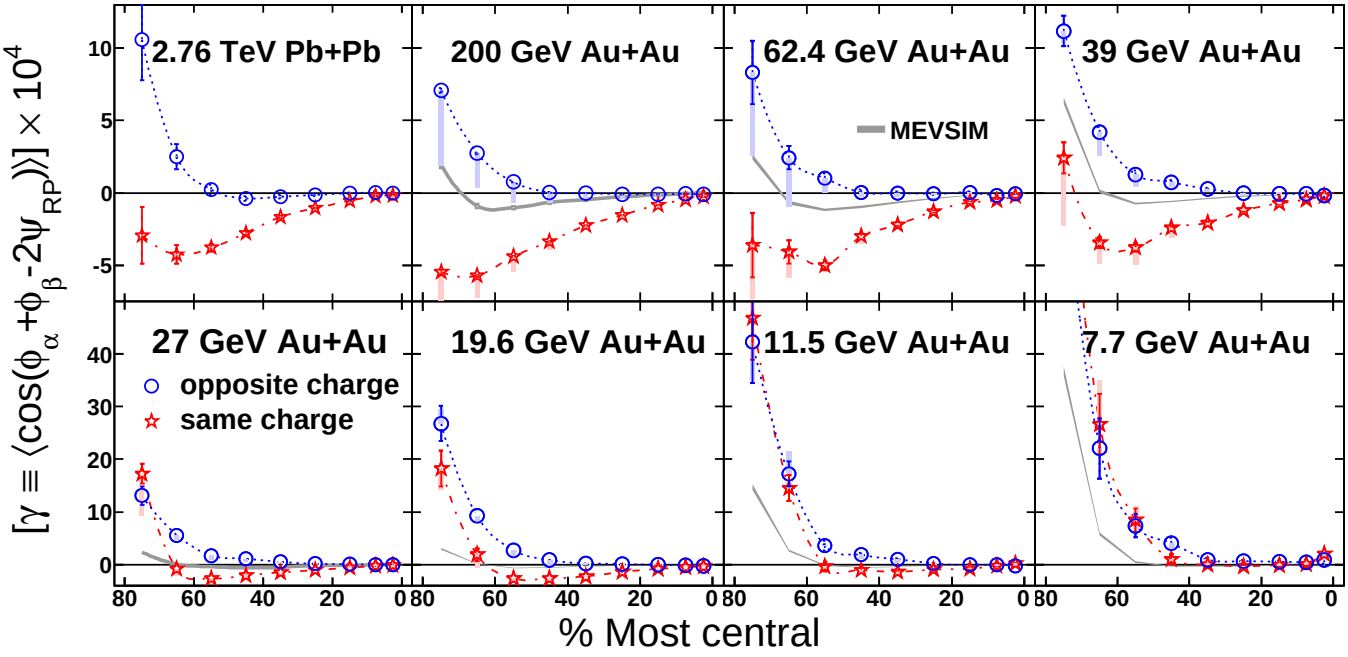

FIG. 7: Three-point correlator as a function of centrality for Au+Au collisions at 7.7-200 GeV [56], and for Pb+Pb collisions at 2.76 TeV [49]. Note that the vertical scales are different for different rows. The systematic errors (grey bars) bear the same meaning as in Fig. 6. Charge independent results from the model calculations of MEVSIM [51] are shown as grey curves.

A further understanding of the origin of the observed charge separation could be achieved with a study of the beam-energy dependence of the correlation. The charge separation effect depends strongly on the formation of the quark gluon plasma and chiral symmetry restoration [1], and the signal can be greatly suppressed or completely absent at low collision energies where a QGP has significantly shortened lifetime or not even formed. Taking into account that the lifetime of the strong magnetic field is larger at smaller collision energies, this could lead to an almost threshold effect: with decreasing collision energy, the signal might slowly increase with an abrupt drop thereafter. Unfortunately, the exact energy dependence of the CME is not calculated yet.

Figure 7 presents γ_{OS} and γ_{SS} correlators as functions of centrality for Au+Au collisions at $\sqrt{s_{NN}} = 7.7 - 200$ GeV measured by STAR [56], and for Pb+Pb collisions at 2.76 TeV by ALICE [49]. In most cases, the difference between γ_{OS} and γ_{SS} is still present with the "right" ordering, manifesting extra charge-separation fluctuations perpendicular to the reaction plane. With decreased beam energy, both γ_{OS} and γ_{SS} tend to rise up starting from peripheral collisions. This feature seems to be charge independent, and can be explained by momentum conservation and elliptic flow [43]. Momentum conservation forces all produced particles, regardless of charge, to separate from each other, while elliptic flow works in the opposite sense. For peripheral collisions, the multiplicity (N) is small, and momentum conservation dominates. The lower beam energy, the smaller N, and the higher γ_{OS} and γ_{SS}. For more central collisions where the multiplicity is large enough, this type of charge-independent background can be estimated with $-v_2/N$ [43, 57]. MEVSIM is a Monte Carlo event generator developed for STAR simulations [51]. In Fig. 7, we also show the model calculations of MEVSIM with the implementation of v_2 and momentum conservation, which qualitatively describe the beam-energy dependence of the charge-independent background. The difference between γ_{OS} and γ_{SS} seems to vanish at low collision energies, but the interpretation involves an ambiguity to be discussed in the Sec III B.

B. Flow Backgrounds

The γ correlator by construction contains the background terms $B_{\rm IN}$ and $B_{\rm OUT}$, and their difference was originally studied for the "flowing cluster" case [44]:

$$\frac{B_{\rm IN}-B_{\rm OUT}}{B_{\rm IN}+B_{\rm OUT}} \approx v_{2,\rm cl}\frac{\langle\cos(\phi_\alpha+\phi_\beta-2\phi_{\rm cl})\rangle}{\langle\cos(\phi_\alpha-\phi_\beta)\rangle}, \tag{6}$$

where $\phi_{\rm cl}$ is the cluster emission azimuthal angle, and ϕ_α and ϕ_β are the azimuthal angles of two decay products. The flowing cluster can be generalized to a larger portion of or even the whole event, through the mechanisms of transverse momentum conservation (TMC) [58, 59] and/or local charge conservation (LCC) [60]. One useful tool to study the background is the two-particle correlator, $\delta \equiv \langle\cos(\phi_\alpha-\phi_\beta)\rangle$, which ideally should be protortional to $\langle a_{1,\alpha}a_{1,\beta}\rangle$, but in reality is dominated by backgrounds. For example, the TMC effect leads to the following pertinent correlation terms in δ and γ [59]:

$$\delta \;\to\; -\frac{1}{N}\frac{\langle p_T\rangle_\Omega^2}{\langle p_T^2\rangle_{\rm F}}\frac{1+(\bar v_{2,\Omega})^2-2\bar v_{2,\rm F}\bar v_{2,\Omega}}{1-(\bar v_{2,\rm F})^2}, \tag{7}$$

$$\gamma \;\to\; -\frac{1}{N}\frac{\langle p_T\rangle_\Omega^2}{\langle p_T^2\rangle_{\rm F}}\frac{2\bar v_{2,\Omega}-\bar{\bar v}_{2,\rm F}-\bar{\bar v}_{2,\rm F}(\bar v_{2,\Omega})^2}{1-(\bar{\bar v}_{2,\rm F})^2} \approx \kappa\cdot v_{2,\Omega}\cdot\delta, \tag{8}$$

where $\kappa = (2\bar v_{2,\Omega}-\bar{\bar v}_{2,\rm F})/v_{2,\Omega}$, and $\bar v_2$ and $\bar{\bar v}_2$ represent the p_T- and p_T^2-weighted moments of v_2, respectively. The subscript "F" denotes an average of all produced particles in the full phase space; the actual measurements will be only in a fraction of the full space, denoted by "Ω". The background contribution due to the LCC effect has a similar characteristic structure as the above [58, 60].

It is convenient to express γ and δ with a two-component framework [56, 59]:

$$\gamma \;\equiv\; \langle\langle\cos(\phi_\alpha+\phi_\beta-2\Psi_{\rm RP})\rangle\rangle = \kappa v_2 B - H, \tag{9}$$

$$\delta \;\equiv\; \langle\langle\cos(\phi_\alpha-\phi_\beta)\rangle\rangle = B + H, \tag{10}$$

where H and B are the CME and background contributions, respectively. The background-subtracted correlator, H, can be obtained from the ensemble averages of several observables:

$$H^\kappa = (\kappa v_2\delta-\gamma)/(1+\kappa v_2). \tag{11}$$

The major uncertainty in the above expression, the coefficient κ, depends on particle charge combination and particle transverse momentum. It may also depend on centrality and collision energy, reflecting slightly different particle production mechanism in different conditions.

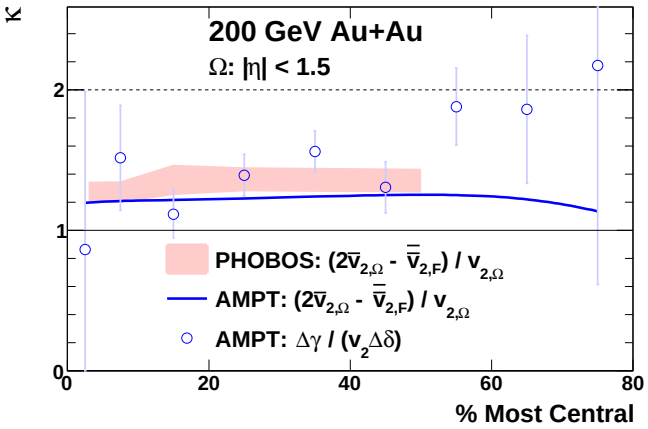

FIG. 8: Estimation of κ with three approaches for 200 GeV Au+Au [61].

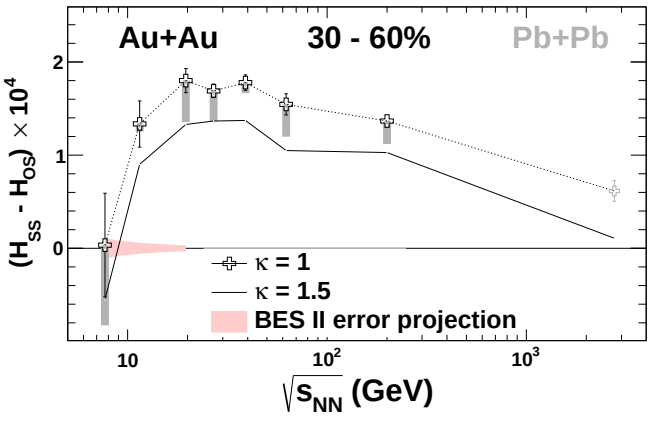

FIG. 9: ΔH as a function of beam energy for 30−60% Au+Au (Pb+Pb) collisions [49, 56]. The systematic errors (grey bars) bear the same meaning as in Fig. 6.

Figure 8 shows the κ values estimated for Au+Au collisions at 200 GeV [61], with the v_2 measurements by the PHOBOS collaboration [62, 63], and with the v_2 calculations from the AMPT model [64–66]. Here only the TMC

effect has been taken in account, and κ is typically within $[1.2, 1.4]$ for $|\eta| < 1.5$. The κ values attained this way will vary slightly if a smaller $|\eta|$ acceptance is involved. In reality, κ should be averaged over various mechanisms such as TMC, LCC and resonance decays. The AMPT model gives a more comprehensive estimate in Fig. 8 via $\Delta\gamma/(v_2\Delta\delta)$, where the numerator is solely due to flow backgrounds. For the centrality range of $10-50\%$, where the statistical uncertainties are small, the κ values thus obtained are close to those estimated with the v_2 information.

Figure 9 shows $(H_{\rm SS}^{\kappa=1} - H_{\rm OS}^{\kappa=1})$ as a function of beam energy for $30-60\%$ Au+Au (Pb+Pb) collisions [49, 56]. $\Delta H^{\kappa=1.5}$ is depicted with the solid line. In both cases of κ, ΔH demonstrates a weak energy dependence above 19.6 GeV, and tends to diminish from 19.6 to 7.7 GeV, though the statistical errors are large for 7.7 GeV. This may be explained by the probable domination of hadronic interactions over partonic ones at low energies. A more definitive conclusion may be reached with a more accurate estimation of κ and with higher statistics at lower energies in the proposed phase II of the RHIC Beam Energy Scan program, as illustrated by the shaded band in Fig. 9.

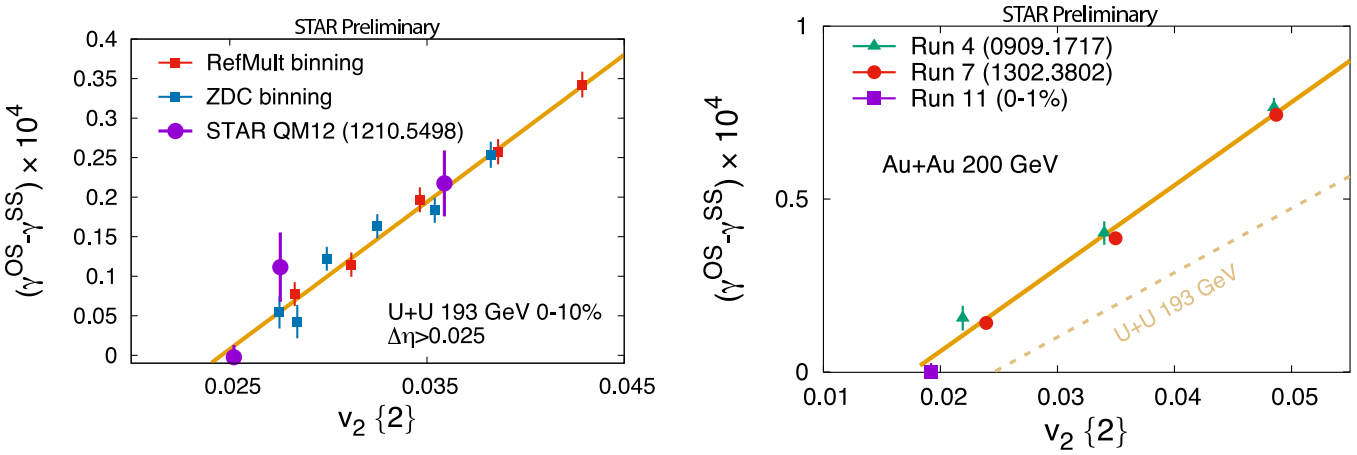

FIG. 10: $\Delta\gamma$ as a function of v_2 for various centrality selections within the $0-10\%$ centrality range in U+U collisions (left) and Au+Au collisions (right). [70–72]

Uranium nuclei have been collided at RHIC in order to study the dependence of multiplicity production, flow, and the CME on the initial overlap geometry [67, 68]. Early ideas hold that the prolate shape of Uranium nuclei would make it possible to select nearly fully overlapping events with large elliptic flow values, but with small magnetic fields. However, owing to fluctuations, the square of the magnetic field is not particularly small. Measurements of very central collisions also demonstrated that the number of produced particles does not depend as strongly on the configuration of the collisions as anticipated in the two-component multiplicity model, leaving the experiments with a significantly reduced ability to independently manipulate the flow and the magnetic field [69].

Figure 10 shows measurements of $\Delta\gamma \equiv \gamma_{\rm OS} - \gamma_{\rm SS}$ for the $0-10\%$ centrality range in 193 GeV U+U (left) and 200 GeV Au+Au collisions (right) [70–72]. In both U+U and Au+Au collisions, the signal increases roughly with v_2. This initial observation may suggest that the charge-separation observable is dominated by a v_2 dependence. However, the charge separation goes to zero while v_2 is still sizable in central Au+Au and central U+U collisions. Model calculations show that the quantity $\left\langle (eB/m_\pi^2)^2 \cos[2(\Psi_B - \Psi_{\rm RP})] \right\rangle$ as a function of eccentricity exhibits the same trend [71]: although $\langle B^2 \rangle$ remains large owing to fluctuations, $\langle \cos[2(\Psi_B - \Psi_{\rm RP})] \rangle$ goes to zero as Ψ_B and $\Psi_{\rm RP}$ become decorrelated in very central collisions. So while fluctuations in central collisions force the participant eccentricity (positive-definite) away from zero, the decorrelation of Ψ_B and $\Psi_{\rm RP}$ drives $\left\langle (eB/m_\pi^2)^2 \cos[2(\Psi_B - \Psi_{\rm RP})] \right\rangle$ to zero. The data therefore appear to be in better agreement with a CME interpretation than a flow background interpretation. A phenomenological study for extrapolating both signal and background from Au+Au to U+U collisions was done in Ref. [73].

Another measurement that can clarify the origin of the charge-dependent correlations and the role of the background was suggested [74]: the correlations measured with respect to the $4^{\rm th}$ harmonic event plane, $\langle \cos(2\phi_\alpha + 2\phi_\beta - 4\Psi_{\rm RP}) \rangle$, should not contain any contribution from the CME, but it should include the effect of the flow-related background. The correlations due to the background in this case are expected to be somewhat smaller in magnitude as the $4^{\rm th}$ harmonic flow is not that strong as the elliptic flow. The preliminary results of such measurements by ALICE are presented in Fig. 11 [75] with the same-charge and opposite-charge pair correlations relative to the $4^{\rm th}$ harmonic event plane as functions of centrality (left), and the charge-dependent parts with respect to the $2^{\rm nd}$ and $4^{\rm th}$ harmonic event planes (right). The correlations relative to the $4^{\rm th}$ harmonic event plane are very weak and suggestive of small background contributions. Detailed simulations have to be performed to draw more definite conclusion from this measurement.

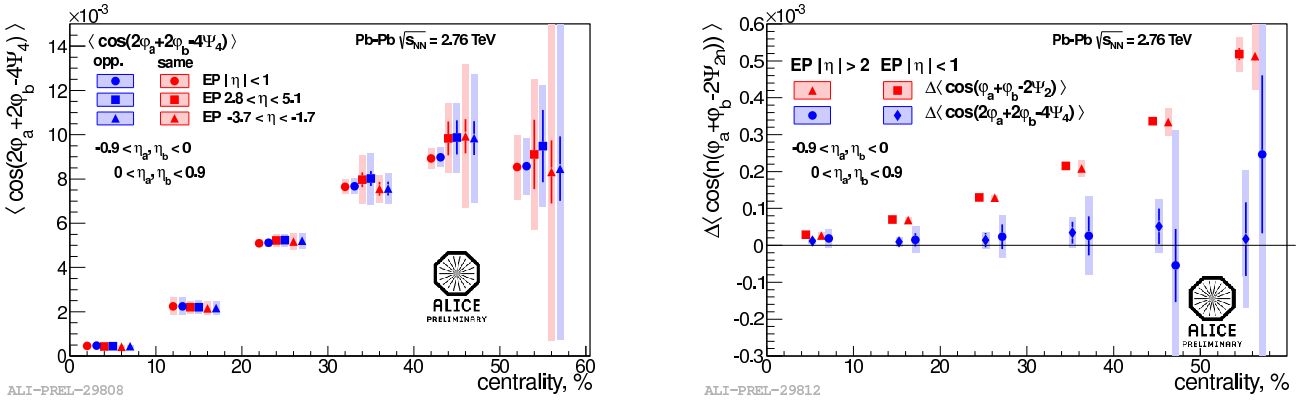

FIG. 11: (Left panel) Same-charge and opposite-charge pair correlations relative to the 4$^{\text{th}}$ harmonic event plane as functions of centrality. (Right panel) Comparison of the charge-dependent parts in correlations with respect to the 2$^{\text{nd}}$ and 4$^{\text{th}}$ harmonic event planes. [75]

IV. CHIRAL VORTICAL EFFECT

The Chiral Vortical Effect (CVE) is related to the CME, and its experimental manifestation is the baryonic charge separation, instead of the electric charge separation, perpendicular to the reaction plane. As a result, the three-point γ correlator is still applicable, only now between two (anti)baryons. However, if both particles are (anti)protons that carry also electric charges, there will be an ambiguity due to the possible signal arising from the CME. The study of the γ correlator with an electrically neutral baryon, such as Λ, will provide more conclusive evidence for the baryonic charge separation effect.

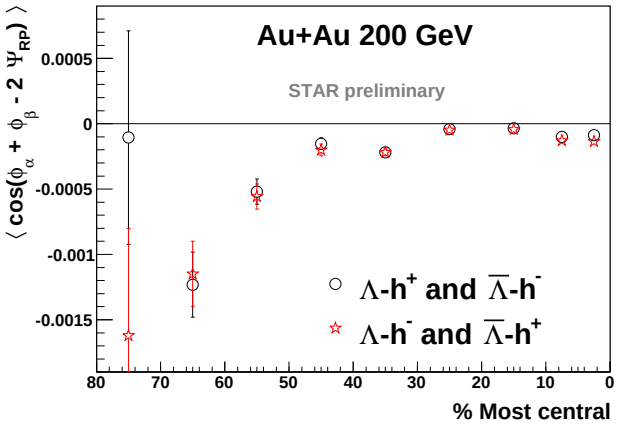

FIG. 12: γ correlation of Λ-h^+ ($\bar{\Lambda}$-h^-) and Λ-h^- ($\bar{\Lambda}$-h^+) as functions of centrality in Au+Au collisions at 200 GeV [54].

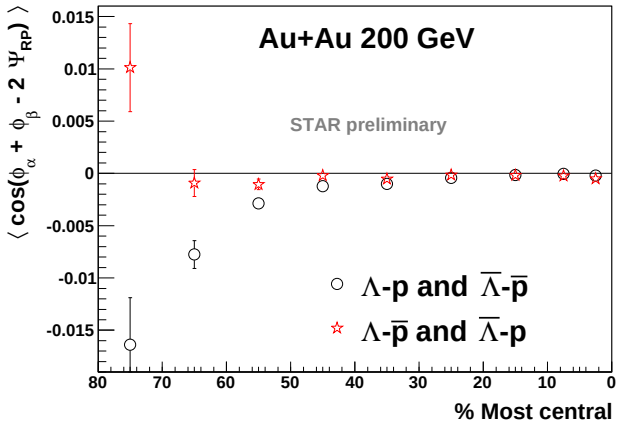

FIG. 13: γ correlation of Λ-p ($\bar{\Lambda}$-$\bar{p}$) and Λ-$\bar{p}$ ($\bar{\Lambda}$-p) as functions of centrality in Au+Au collisions at 200 GeV [54].

Although (anti)Λ's are electrically neutral, it is still a question whether the strange quarks behave the same way as the up/down quarks in the chiral dynamics during the collision. If the answer is no, then (anti)Λ's may still act like electrically charged particles in the γ correlation. Figure 12 shows the γ correlation of Λ-h^+ ($\bar{\Lambda}$-h^-) and Λ-h^- ($\bar{\Lambda}$-h^+) as functions of centrality in Au+Au collisions at 200 GeV [54]. Note that (anti)protons have been excluded from the charged hadrons in the correlation to avoid any possible CVE contribution. Tentatively assuming Λs ($\bar{\Lambda}$s) are positively(negatively)-charged, we find that the "same-charge" and "opposite-charge" correlations are consistent with each other, which means no charge-dependent effect. The message is twofold: first, from the $K^0_S - h$ correlations [54] we learn that the different behaviors of same-charge and opposite-charge particle correlations as shown in Fig. 5 are really due to the electric charge, and therefore the null charge-separation effect in Λ-h indicates that (anti)Λs manifest no electric charges in the γ correlation. So the strange quarks inside seem to behave the same way as the up/down quarks in the chiral dynamics. Second, the Λ-h correlation provides a baseline check for the Λ-p correlation, and any possible signal in the latter should not come from the CME contribution.

Figure 13 shows γ correlation of Λ-p ($\bar{\Lambda}$-$\bar{p}$) and Λ-$\bar{p}$ ($\bar{\Lambda}$-p) as functions of centrality in Au+Au collisions at 200 GeV [54]. The same-baryonic-charge correlation has a different behavior from the opposite-baryonic-charge correlation from mid-central to peripheral collisions. This baryonic charge separation with respect to the event plane is consistent with the expectation from the CVE. More investigations into the background contribution are needed. For example, in analog with the local charge conservation, there could be the local baryonic charge conservation that plays a similar role as LCC when coupled to v_2. The magnitudes of the Λ-p correlations are much larger than those of the h-h correlations. This is partially because the $\langle p_T \rangle$ of baryons is higher than that of mesons, and the correlation strength increases with the average p_T of the two particles in the correlation. A future differential measurement vs the pair average p_T and further correlations between identified particles may provide a better comparison of the correlation strength between the CME- and CVE-related correlations.

V. CHIRAL MAGNETIC WAVE

The CMW is a signature of the chiral symmetry restoration in the QGP, and consists of actually two chiral gapless modes traveling at the same speed [11]: the right-handed (left-handed) wave transports the right-handed (left-handed) density and current in the direction parallel (antiparallel) to the $\overrightarrow{B}$ direction. A more general analysis [76] studied various possible collective modes based on a non-neutral-background QGP (i.e. with nonzero μ and/or μ_5) in external electric and/or magnetic fields, and found a new type of collective motion, the chiral electric wave (CEW), arising from CESE and propagating in parallel/antiparallel to the $\overrightarrow{E}$ field. In symmetric collisions there should be no net electric field on average, but asymmetric collisions like Cu+Au could provide a test ground for the CEW measurements.

A. Electric quadrupole observable

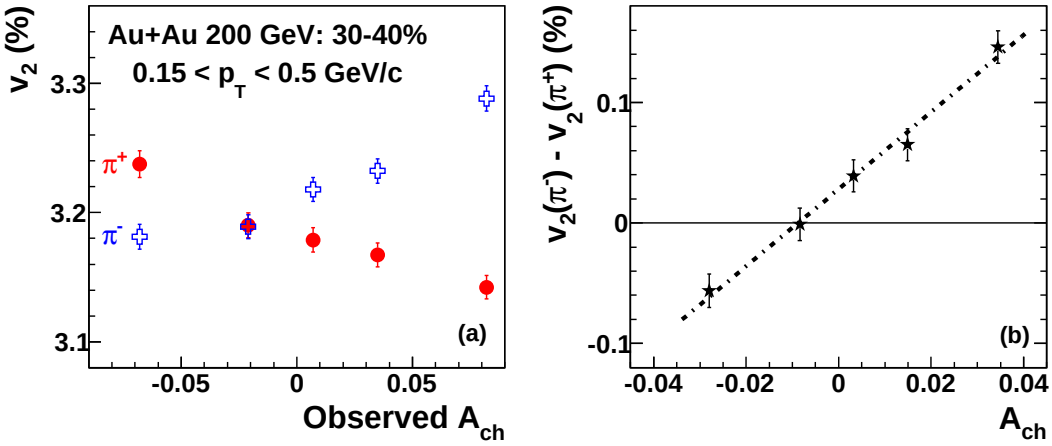

FIG. 14: (a) pion v_2 as a function of observed charge asymmetry and (b) v_2 difference between π^- and π^+ as a function of charge asymmetry with the tracking efficiency correction, for 30-40% Au+Au collisions at 200 GeV [79].

The CMW will induce a finite electric quadrupole moment of the collision system, with additional positive (negative) charge at the "poles" ("equator") of the produced fireball [11]. This electric quadrupole, if boosted by radial flow, will lead to charge-dependent elliptic flow. Taking pions as an example, on top of the baseline $v_2^{\rm base}(\pi^{\pm})$, the CMW will lead to [11]

$$v_2(\pi^{\pm}) = v_2^{\rm base}(\pi^{\pm}) \mp (\frac{q_e}{\bar{\rho}_e}) A_{\rm ch}, \tag{12}$$

where q_e, $\bar{\rho}_e$ and $A_{\rm ch} = (N_+ - N_-)/(N_+ + N_-)$ are the quadrupole moment, the net charge density and the charge asymmetry of the collision event, respectively. As $\langle A_{\rm ch} \rangle$ is always positive, the $A_{\rm ch}$-integrated v_2 of π^- (π^+) should be above (below) the baseline owing to the CMW. However, the baseline v_2 may be different for π^+ and π^- because of several other physics mechanisms [77, 78]. Therefore, it is less ambiguous to study the CMW via the $A_{\rm ch}$ dependence of pion v_2 than via the $A_{\rm ch}$-integrated v_2.

Taking 30-40% 200 GeV Au+Au for example, pion v_2 is shown as a function of $A_{\rm ch}$ in panel (a) of Fig. 14 [79]. π^- v_2 increases with $A_{\rm ch}$ while π^+ v_2 decreases with a similar magnitude of the slope. Note that v_2 was integrated over a narrow low p_T range ($0.15 < p_T < 0.5$ GeV/c) to focus on the soft physics of the CMW. Such a p_T selection also makes sure that the $\langle p_T \rangle$ is independent of $A_{\rm ch}$ and is the same for π^+ and π^-, so that the v_2 splitting is not a trivial effect due to the $\langle p_T \rangle$ variation. This v_2 splitting was also confirmed by ALICE results for Pb+Pb collisions at 2.76 TeV [80]. The v_2 difference between π^- and π^+ is fitted with a straight line in panel (b). The slope parameter r, or presumably $2q_e/\bar{\rho}_e$ from Eq. 12, is positive and qualitatively consistent with the expectation of the CMW picture. The fit function is nonzero at $\langle A_{\rm ch} \rangle$, indicating the $A_{\rm ch}$-integrated v_2 for π^- and π^+ are different, which was also observed in Ref. [81].

The same procedure as above was followed by STAR to retrieve the slope parameter r as a function of centrality for Au+Au collisions at 200, 62.4, 39, 27, 19.6, 11.5 and 7.7 GeV, as shown in Fig. 15 [79]. A similar rise-and-fall trend is observed in the centrality dependence of the slope parameter for all the beam energies except 11.5 and 7.7 GeV, where the slopes are consistent with zero with large statistical uncertainties. It was argued [77] that at lower beam energies the $A_{\rm ch}$-integrated v_2 difference between particles and anti-particles can be explained by the effect of quark transport from the projectile nucleons to mid-rapidity, assuming that the v_2 of transported quarks is larger than that of produced ones. The same model, however, when used to study $v_2(\pi^-) - v_2(\pi^+)$ as a function of $A_{\rm ch}$, suggested a negative slope [82], which is contradicted by the data.

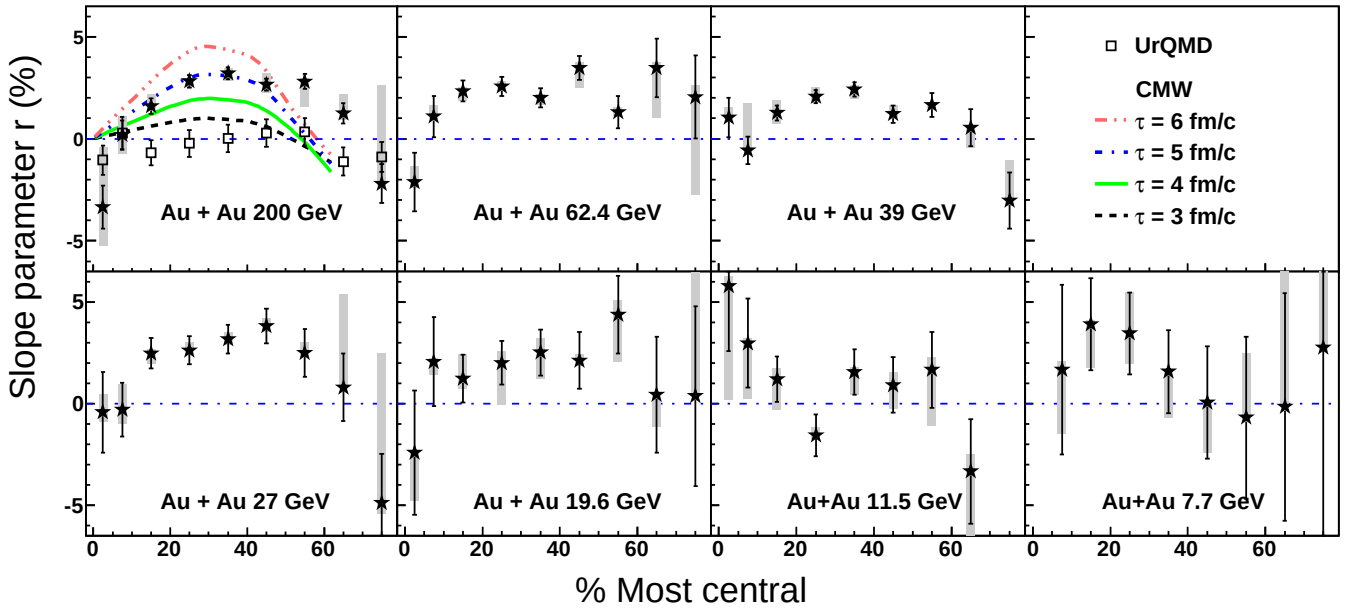

FIG. 15: The slope parameter r as a function of centrality for Au+Au collisions at 7.7-200 GeV [79]. The grey bands represent the systematic errors. For comparison, we also show the UrQMD calculations [52] and the calculations of the CMW [83] with different duration times.

To check if the observed slope parameters come from conventional physics, the same analysis of the Monte Carlo events from UrQMD [52] was carried out. For Au+Au collisions at 200 GeV, the slopes extracted from UrQMD events are consistent with zero for the 10-70% centrality range, where the signal from the real data is prominent. Similarly, the AMPT event generator [64, 65] also yields slopes consistent with zero (not shown here). On the other hand, the simplified CMW calculations [83] demonstrate a centrality dependence of the slope parameter similar to the data. Recently a more realistic implementation of the CMW [84] confirmed that the CMW contribution to r is sizable, and the centrality dependence of r is qualitatively similar to the data. A quantitative comparison between data and theory requires further work on both sides to match the kinematic regions used in the analyses. For example, the measured $A_{\rm ch}$ only represents the charge asymmetry of a pseudorapidity slice ($|\eta| < 1$) of an event, instead of that of the whole collision system. We expect $A_{\rm ch}$ for these two cases to be proportional to each other, but the determination of the ratio will be model dependent.

Figure 16 shows a comparison in the slope parameter r between STAR results for 200 GeV Au+Au [79] and ALICE results for 2.76 TeV Pb+Pb [80]. Overall, the slopes are surprisingly similar when considering the different collision energies and multiplicities, as well as the different kinematic acceptance: the STAR data estimated v_2 for charged pions with $0.15 < p_T < 0.5$ GeV/c and $|\eta| < 1$, while the ALICE data are for unidentified hadrons with $0.2 < p_T < 5$

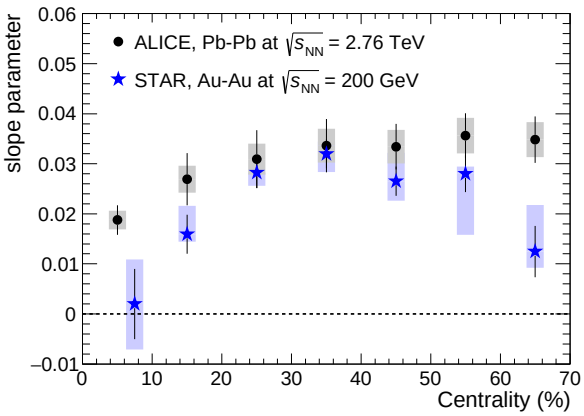

FIG. 16: Slope parameter r as a function of centrality for 200 GeV Au+Au [79] and 2.76 TeV Pb+Pb [80]. Statistical (systematic) uncertainties are indicated by vertical bars (shaded boxes).

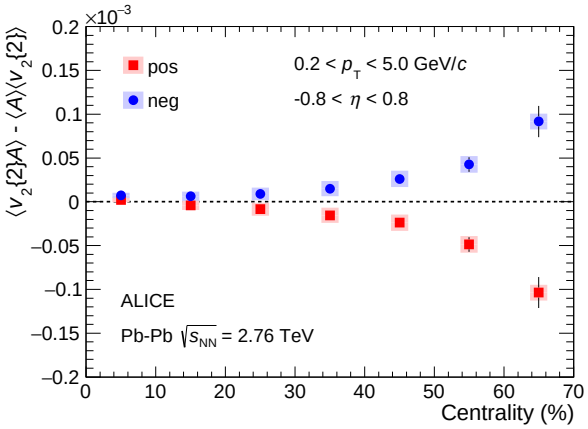

FIG. 17: Three-particle correlator for the second harmonic, for positive (red squares) and negative (blue circles) particles for 2.76 TeV Pb+Pb [80]. Statistical (systematic) uncertainties are indicated by vertical bars (shaded boxes).

GeV/c and $|\eta| < 0.8$.

One drawback with the measurement of $v_2(A_{\rm ch})$ is that the observed $A_{\rm ch}$ requires a correction factor due to the finite detector tracking efficiency. A novel correlator [85] that is independent of efficiency was proposed,

$$\langle\langle\cos[n(\phi_1-\phi_2)]q_3\rangle\rangle = \langle\cos[n(\phi_1-\phi_2)]q_3\rangle - \langle\cos[n(\phi_1-\phi_2)]\rangle\langle q_3\rangle. \quad (13)$$

Here ϕ_1 and ϕ_2 are the azimuthal angles of particles 1 and 2, and q_3 is the charge (±1) of particle 3. The single brackets represent the average over particles and events, and the double bracket denotes the cumulant. In the absence of charge dependent correlations, the correlator should be equal to zero. Note that when the charge of the third particle is averaged over all particles in the event (in the specified kinematic acceptance), the mean is equal to the charge asymmetry, i.e. $\langle q_3\rangle = A_{\rm ch}$.

The three-particle correlator (as in Eq. 13) for the 2$^{\rm nd}$ harmonic was measured by ALICE and is presented in Fig. 17 as a function of centrality in Pb+Pb collisions at 2.76 TeV GeV [80]. A substantial increase in the correlation strength is seen as the collisions become more peripheral, which can be caused by a combination of several factors. For example, the magnetic field strength increases as the impact parameter increases, and this would cause the stronger correlations due to the CMW. Additionally, the LCC effect could play a role [85], and neither of these necessarily comes at the expense of the other; in principle the observable could have contributions from both of these and/or additional contributions from as yet unknown sources of correlation.

B. Possible backgrounds

It was pointed out in Ref. [86] that local charge conservation at freeze-out, when convoluted with the characteristic shape of $v_2(\eta)$ and $v_2(p_T)$, may provide a qualitative explanation for the finite v_2 slope observed from data. A realistic estimate of the contribution of this mechanism turns out to be smaller than the measurment by an order of magnitude [79]. Ref. [86] also proposes a test with the v_3 measurement, and the corresponding slope parameters for v_3 were reported by STAR to be consistent with zero [87], which further suggests the smallness of this effect. ALICE measured the three-particle correlator multiplied by $\langle dN_{\rm ch}/d\eta\rangle$ for the 3$^{\rm rd}$ harmonic and the 4$^{\rm th}$ harmonic [80]. In both cases, the centrality dependence of the charge dependence is flat, in contrast to the 2$^{\rm nd}$ harmonic that has a significant centrality dependence. This may suggest a different nature of the correlation, or reflect a weaker centrality dependence of v_3 compared with that of v_2. Future measurements of these higher harmonics with better precision will shed light on the true origin of this correlator.

A recent hydrodynamic study [88] suggested that simple viscous transport of charges, combined with certain specific initial conditions, might lead to a sizable contribution to the observed v_2 splitting of charged pions. In order for the results of pion splitting to resemble data, the authors had to assume a crucial relation between isospin chemical potential and the electric charge asymmetry, which needs to be verified. Furthermore, certain predictions of this model (e.g. splitting for kaons) appear to be not in line with current experimental information [89]. Clearly whether

such an idea works or not, would need to be thoroughly vetted by realistic viscous hydrodynamic simulations. But all that said, this study poses a very important question: to make a firm case for the observation of anomalous charge transport via the CMW, the normal (viscous hydrodynamical) transport of charges should be quantitatively understood.

VI. FUTURE MEASUREMENTS

The confirmation of the experimental observation of several chiral anomalous effects will bring forth an exciting program to directly study the non-perturbative sector of QCD. Future experimental measurements should aim at more detailed study of the observed signals as well as understanding the background effects. Previous sections have covered a few such topics: initial magnetic field and vorticity, correlations with identified particles, higher-harmonic correlations, BES-II and U+U collisions. In the following, we will focus on the event-shape engineering (ESE) and isobaric collisions.

A. Event shape engineering

Flow-related backgrounds could be potentially removed via ESE [68, 90], with which *spherical* events or sub-events are selected, so that the particles of interest therein carry zero v_2. A previous attempt was made with the charge-separation observable of CMAC (roughly equivalent to γ), as a function of event-by-event "observed v_2" [55]. However, there are several issues in this approach that prevent a clear interpretation of the result. Ref. [61] studied the flow vector $\overrightarrow{q} = (q_x^{\rm A}, q_y^{\rm A})$ of the sub-event of interest, A:

$$q_x^{\rm A} = \frac{1}{\sqrt{N}} \sum_i^N \cos(2\phi_i^{\rm A}) \tag{14}$$

$$q_y^{\rm A} = \frac{1}{\sqrt{N}} \sum_i^N \sin(2\phi_i^{\rm A}), \tag{15}$$

and found that q^2 is a good handle on event shape.

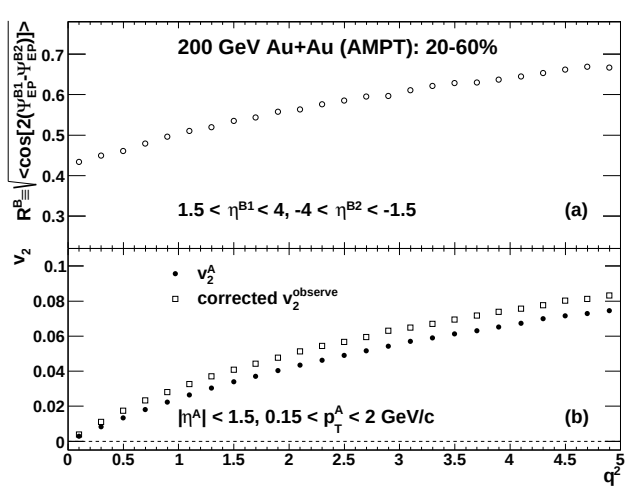

FIG. 18: The sub-event plane resolution (upper), and the true elliptic flow $v_2^{\rm A}$ and the corrected $v_2^{\rm observe}$ as functions of q^2 (lower), from AMPT simulations. [61]

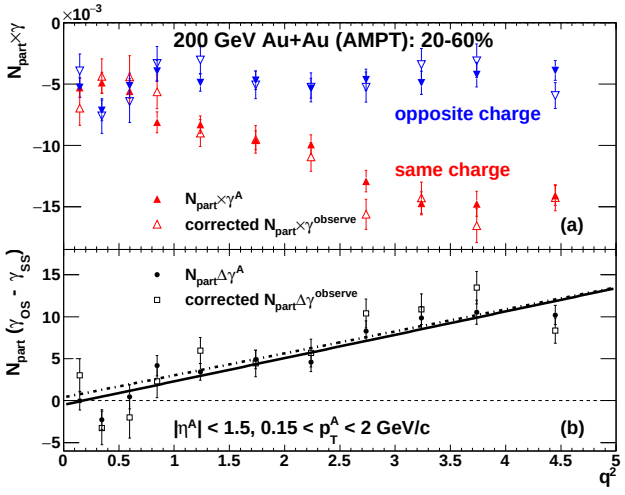

FIG. 19: $N_{\rm part} \times \gamma$ (upper) and $N_{\rm part}\Delta\gamma$ (lower) as functions of q^2, from AMPT simulations. [61] The solid (dashed) line in the lower panel is a linear fit of the full (open) data points.

Figure 18 shows the event plane resolution ($R^{\rm B}$) for the sub-events B1 and B2 (upper), and the true elliptic flow $v_2^{\rm A}$ and the corrected $v_2^{\rm observe}$ as functions of q^2 (lower), from AMPT simulations of $20-60\%$ Au+Au collisions at $\sqrt{s_{\rm NN}} = 200$ GeV [61]. Each AMPT event has been divided into three sub-events according to pseudorapidity, η: sub-event A contains particles of interest with $|\eta| < 1.5$, and sub-event B1(B2) serves as a sub-event plane using

particles with $1.5 < \eta < 4$ ($-4 < \eta < -1.5$). Flow fluctuation causes a positive correlation in flow between sub-events in the same event, and as a result, $R^{\rm B}$ for sub-event B1 (B2) increases with q^2 for sub-event A. The lower panel displays a discrepancy between $v_2^{\rm A}$ and the corrected $v_2^{\rm observe}$, owing to the difference between the reaction plane and the participant plane [91], in terms of non-flow and flow fluctuation. What matters more is the fact that both v_2 values decrease with q^2, and drop to $(0, 0)$, which demonstrates q's capability of selecting spherical sub-events in the second harmonic.

The upper panel of Fig. 19 presents the γ correlators multiplied by the number of participating nucleons, $N_{\rm part}$, as functions of q^2, for $20-60\%$ AMPT events of Au+Au collisions at 200 GeV [61]. For both the same-charge and the opposite-charge correlators, the true $\gamma^{\rm A}$ and the corrected $\gamma^{\rm observe}$ are consistent with each other within the statistical uncertainties. This indicates that compared with v_2, γ is less sensitive to non-flow or flow fluctuation. At larger q^2, the opposite-charge correlators are above the same-charge correlators, suggesting a finite flow-related background. The opposite- and same-charge correlators converge at small q^2. The lower panel shows $N_{\rm part}\Delta\gamma \equiv N_{\rm part}(\gamma_{\rm OS} - \gamma_{\rm SS})$ vs q^2, and again, the two observables seem to coincide. Linear fits to both observables yield small intercepts that are consistent with zero. The finite $\Delta\gamma$ values in AMPT events are solely due to background contributions, so the disappearance of background is demonstrated when the "correctable" observable ($\Delta\gamma$) is projected to zero q^2. Ref. [61] has designed a promising recipe for future measurements to effectively remove flow backgrounds and restore the ensemble average of the CME signal.

B. Isobaric collisions

To disentangle the possible CME signal and the flow-related backgrounds, one can utilize experimental setups to either vary the backgrounds with the signal fixed, or vary the signal with the backgrounds fixed. The former approach was carried out by exploiting the prolate shape of the uranium nuclei [68]. However, it was found that the total multiplicity of detected hadrons is far less dependent on the number of binary collisions than expected [69], so it is very hard to isolate tip-tip collisions (that generate small v_2) from body-body collisions (that generate large v_2). This significantly reduces the lever arm available to manipulate v_2 in order to separate flow backgrounds from the CME.

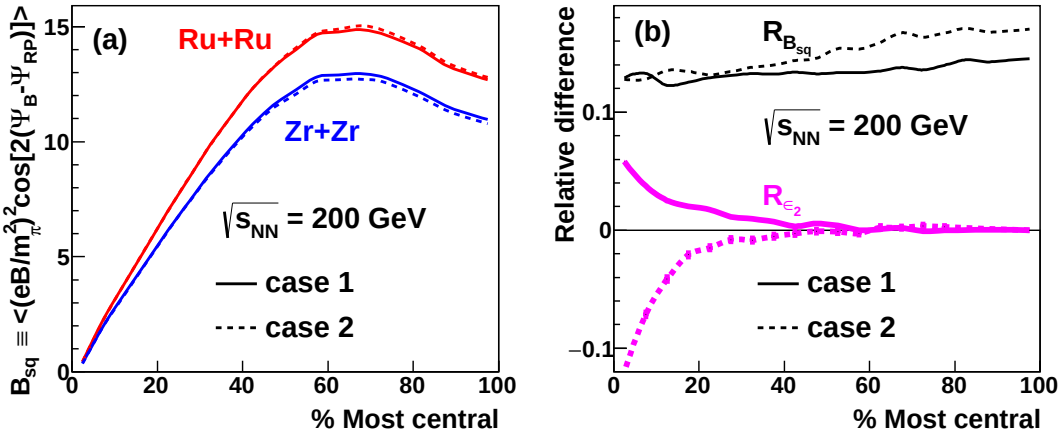

FIG. 20: Theoretical calculation [92] of the initial magnetic field squared with correction from azimuthal fluctuation for Ru+Ru and Zr+Zr collisions at 200 GeV (a) and their relative difference (b) versus centrality. Also shown is the relative difference in initial eccentricity (b). The solid (dashed) lines correspond to the parameter set of case 1 (case 2).

The latter approach (with the v_2-driven backgrounds fixed) can be realized, especially for mid-central/mid-peripheral events, with collisions of isobaric nuclei, such as $^{96}_{44}$Ru and $^{96}_{40}$Zr [68]. Ru+Ru and Zr+Zr collisions at the same beam energy are almost identical in terms of particle production [92], while the charge difference between Ru and Zr nuclei provides a handle on the initial magnetic field. Our current knowledge of the deformity (β_2) of Ru and Zr is incomplete: e-A scattering experiments (case 1) [93, 94] state that Ru is more deformed ($\beta_2^{\rm Ru} = 0.158$) than Zr ($\beta_2^{\rm Zr} = 0.08$), while comprehensive model deductions (case 2) [95] tell the opposite, that $\beta_2^{\rm Ru} = 0.053$ is smaller than $\beta_2^{\rm Zr} = 0.217$. This systematic uncertainty has different impacts on the signal (via the initial magnetic field) and the background (via the initial eccentricity) to be discussed later. As a by-product, v_2 measurements in central collisions will discern which information source is more reliable regarding the deformity of the Zr and Ru nuclei.

Figure 20(a) presents the theoretical calculation [92] of the initial magnetic field squared with correction from azimuthal fluctuation of the magnetic field orientation, $B_{sq} \equiv \left\langle (eB/m_\pi^2)^2 \cos[2(\Psi_{\rm B} - \Psi_{\rm RP})] \right\rangle$ (with m_π the pion mass

and $\Psi_{\rm B}$ the azimuthal angle of the magnetic field), for the two collision systems at 200 GeV, using the HIJING model [96, 97]. B_{sq} quantifies the magnetic field's capability of driving the CME signal in the γ correlator. For the same centrality bin, the Ru+Ru collision produces a significantly stronger magnetic field than Zr+Zr. Panel (b) of Fig. 20 shows that the relative difference in B_{sq} between Ru+Ru and Zr+Zr collisions is approaching 15% (case 1) or 18% (case 2) for peripheral events, and reduces to about 13% (both cases) for central events. Figure 20(b) shows the relative difference in the initial eccentricity, R_{ϵ_2}, obtained from the Monte Carlo Glauber simulation. R_{ϵ_2} is highly consistent with 0 for peripheral events, and goes above (below) 0 for the parameter set of case 1 (case 2) in central collisions, because the Ru (Zr) nucleus is more deformed. The relative difference in v_2 should closely follow that in eccentricity, so for the centrality range of interest, $20-60\%$, the v_2-related backgrounds stay almost the same for Ru+Ru and Zr+Zr collisions. Ref. [92] further carried out the projection for the γ measurements in Ru+Ru and Zr+Zr at 200 GeV (400 million events for each collision type), and concluded that a 5σ significance can be achieved for the relative difference in the observable between the two collision systems, assuming the flow backgrounds take up to two-thirds of the observable. The results strongly suggest that the isobaric collisions can serve as an ideal tool to disentangle the signal of the chiral magnetic effect from the v_2-driven backgrounds. The isobaric collisions may also be used to disentangle the signal of the CMW from background effects.

VII. SUMMARY

The physics of anomalous transport is at the heart of QCD as a non-Abelian gauge theory. The interplay of quantum anomalies with magnetic field and vorticity induces a variety of novel transport phenomena in chiral systems. In heavy-ion collisions, these phenomena make a unique probe to the topological properties of the QGP by measuring the charge dependence of the azimuthal distributions of the produced hadrons. The experimental data from Relativistic Heavy Ion Collider at BNL and the Large Hadron Collider at CERN provide an evidence for the predicted effects, with magnitude consistent with theoretical estimates. There exist known conventional backgrounds to all of these experimental observables. However at present there is no compelling alternative explanation that can describe all of the data without invoking the anomalous chiral effects. Nevertheless, much remains to be done both in experiment and theory to substantiate the existing evidence, and we outlined a few such programs that hopefully will be accomplished in the near future.

Acknowledgments

We thank Huan Huang and other members of the UCLA Heavy Ion Physics Group for discussions. This work is supported by a grant (No. DE-FG02-88ER40424) from U.S. Department of Energy, Office of Nuclear Physics. The authors declare that there is no conflict of interest regarding the publication of this paper.

[1] D. E. Kharzeev, L. D. McLerran and H. J. Warringa, Nucl. Phys. A **803**, 227 (2008).
[2] D. Kharzeev, Phys. Lett. B **633**, 260 (2006).
[3] D. Kharzeev and A. Zhitnitsky, Nucl. Phys. A **797**, 67 (2007).
[4] D. Kharzeev, A. Krasnitz and R. Venugopalan, Phys. Lett. B **545**, 298 (2002).
[5] I. Iatrakis, S. Lin and Y. Yin, Phys. Rev. Lett. **114**, 252301 (2015).
[6] K. Fukushima, D. E. Kharzeev and H. J. Warringa, Phys. Rev. Lett. 104, 212001 (2010).
[7] A. M. Poskanzer and S. Voloshin, Phys. Rev. C **58**, 1671 (1998).
[8] D. E. Kharzeev and D. T. Son, Phys. Rev. Lett. **106** (2011) 062301.
[9] D. T. Son and A. R. Zhitnitsky, Phys. Rev. D **70** 074018 (2004).
[10] M. A. Metlitski and A. R. Zhitnitsky, Phys. Rev. D **72** 045011 (2005).
[11] Y. Burnier, D. E. Kharzeev, J. Liao and H.-U. Yee, Phys. Rev. Lett. **107** 052303 (2011).
[12] G. M. Newman, JHEP **0601** 158 (2006).
[13] X. G. Huang and J. Liao, Phys. Rev. Lett. **110**, 232302 (2013).
[14] Y. Jiang, X. G. Huang and J. Liao, Phys. Rev. D **91**, 045001 (2015).
[15] Y. Jiang, X. G. Huang and J. Liao, Phys. Rev. D **92**, 071501 (2015).
[16] D.E. Kharzeev, J. Liao, S.A. Voloshin and G. Wang, Prog. Part. Nucl. Phys. **88**, 1 (2016).
[17] A. Bzdak, V. Skokov, Phys. Lett. B **710**, 171 (2012).
[18] W.T. Deng, X.G. Huang, Phys. Rev. C **85**, 044907 (2012); Phys. Lett. B **742**, 296 (2015).
[19] J. Bloczynski, X.G. Huang, X. Zhang, J. Liao, Phys. Lett. B **718**, 1529 (2013).
[20] L. McLerran, V. Skokov, Nuclear Phys. A **929**, 184 (2014).

[21] X. Guo, S. Shi, N. Xu, Z. Xu, P. Zhuang. arXiv:1502.04407.
[22] U. Gursoy, D. Kharzeev, K. Rajagopal, Phys. Rev. C **89(5)**, 054905 (2014).
[23] K. Tuchin, Adv. High Energy Phys. **2013**, 490495 (2013).
[24] Y. Hirono, M. Hongo, and T. Hirano, Phys. Rev. C **90**, 021903 (2014).
[25] V. Voronyuk, V. D. Toneev, S. A. Voloshin, and W. Cassing, Phys. Rev. C **90**, 064903 (2014).
[26] L. Adamczyk *et al.* [STAR Collaboration], arXiv:1608.04100.
[27] B. I. Abelev *et al.* [STAR Collaboration], Phys. Rev. Lett. **101**, 252301 (2008).
[28] Y. Jiang, Z.W. Lin, J. Liao, arXiv:1602.06580.
[29] M.I. Baznat, K.K. Gudima, A.S. Sorin, O.V. Teryaev, Phys. Rev. C **93**, 031902 (2016).
[30] F. Becattini *et al.*, arXiv:1501.04468.
[31] F. Becattini, L. Csernai, D.J. Wang, Phys. Rev. C **88 (3)**, 034905 (2013).
[32] S. Floerchinger, U.A. Wiedemann, J. High Energy Phys. **1111**, 100 (2011).
[33] J.H. Gao, B. Qi, S.Y. Wang, Phys. Rev. D **90 (8)**, 083001 (2014).
[34] Isaac Upsal *et al.* [STAR Collaboration], J. Phys.: Conf. Ser. **736**, 012016 (2016).
[35] STAR Collaboration, STAR Note **0598**, https://drupal.star.bnl.gov/STAR/starnotes/public/sn0598.
[36] A.H. Tang and G. Wang, Phys. Rev. C **94**, 024920 (2016).
[37] Y. Hirono, D. E. Kharzeev, and Y. Yin, Phys. Rev. D **92**, 125031 (2015).
[38] A. Ipp, A. Di Piazza, J. Evers, and C. H. Keitel, Phys. Lett. B **666**, 315 (2008).
[39] K. A. Mamo and H. U. Yee, Phys. Rev. D **88**, 114029 (2013).
[40] Z.-T. Liang and X.-N. Wang, Phys. Rev. Lett. **94**, 102301 (2005).
[41] M. Baznat, K. Gudima, A. Sorin, and O. Teryaev, Phys. Rev. C **88**, 061901 (2013).
[42] W.-T. Deng and X.-G. Huang, Phys. Rev. C **93**, 064907 (2016)
[43] L. Adamczyk *et al.* [STAR Collaboration], Phys. Rev. C **88** 064911 (2013).
[44] S. A. Voloshin, Phys. Rev. C **70**, 057901 (2004) [hep-ph/0406311].
[45] B. I. Abelev *et al.* [STAR Collaboration], Phys. Rev. Lett. **103** 251601 (2009).
[46] 7. I. Abelev *et al.* [STAR Collaboration], Phys. Rev. C **81** 54908 (2010).
[47] A. Bzdak, V. Koch and J. Liao, Phys. Rev. C **81** 031901 (2010).
[48] N. N. Ajitanand, S. Esumi, R. A. Lacey (PHENIX Collaboration), in: Proc. of the RBRC Workshops, vol.**96**, 230 (2010): "P- and CP-odd ects in hot and dense matter".
[49] B. I. Abelev *et al.*[ALICE Collaboration], Phys. Rev. Lett. **110** 021301 (2013).
[50] N. N. Ajitanand, R. A. Lacey, A. Taranenko and J. M. Alexander, Phys. Rev. C **83** 011901 (2011).
[51] R. L. Ray and R. S. Longacre, arXiv:nucl-ex/0008009.
[52] S. A. Bass *et al.*, Prog. Part. Nucl. Phys. **41** 255 (1998).
[53] M. Gyulassy and X.-N. Wang, Comput. Phys. Commun. **83** 307 (1994);X.N. Wang and M.Gyulassy, Phys. Rev. D **44** 3501 (1991).
[54] F. Zhao (STAR Collaboration), Nucl. Phys. A **931** (2014) 746.
[55] L. Adamczyk *et al.* [STAR Collaboration], Phys. Rev. C **89**, 044908 (2014).
[56] L. Adamczyk *et al.* [STAR Collaboration], Phys. Rev. Lett. **113** (2014) 052302.
[57] A. Bzdak, V. Koch and J. Liao, Phys. Rev. C **83** 014905 (2011).
[58] S. Pratt, S. Schlichting and S. Gavin, Phys. Rev. C **84**, 024909 (2011).
[59] A. Bzdak, V. Koch and J. Liao, Lect. Notes Phys. **871** 503 (2013) [arXiv:1207.7327 [nucl-th]].
[60] S. Schlichting and S. Pratt, Phys. Rev. C **83**, 014913 (2011).
[61] F. Wen, L. Wen and G. Wang, arXiv:1608.03205.
[62] B. alver *et al.* [PHOBOS Collaboration], Phys. Rev. C **83**, 024913 (2011).
[63] B.B Back *et al.* [PHOBOS Collaboration], Phys. Rev. C **72**, 051901(R) (2005).
[64] B. Zhang, C.M. Ko, B.-A. Li and Z.-W. Lin, Phys. Rev. C **61**, 067901 (2000).
[65] Z.-W. Lin, C.M. Ko, B.-A. Li and B. Zhang, Phys. Rev. C **72**, 064901 (2005).
[66] Z.-W. Lin and C.M. Ko, Phys. Rev. C **65**, 034904 (2002);
[67] A. J. Kuhlman and U. W. Heinz, Phys. Rev. C **72**, 037901 (2005).
[68] S. A. Voloshin, Phys. Rev. Lett. **105**, 172301 (2010).
[69] L. Adamczyk *et al.* [STAR Collaboration], Phys. Rev. Lett. **115**, 222301 (2015).
[70] Gang Wang *et al.* [STAR Collaboration], Nucl. Phys A **904-905**, 248c (2013).
[71] P. Tribedy [STAR Collaboration], "Charge sensitive cumulants and flow in U+U collisions", Workshop on Chirality, Vorticity and Magnetic Field in Heavy Ion Collisions, 2016; http://starmeetings.physics.ucla.edu/sites/default/files/pritwish_tribedy.pdf.
[72] V. Skokov, P. Sorensen, V. Koch, S. Schlichting, J. Thomas, S. Voloshin, G. Wang and H.-U. Yee, arXiv:1608.00982.
[73] J. Bloczynski, X. G. Huang, X. Zhang and J. Liao, Nucl. Phys. A **939**, 85 (2015).
[74] S. A. Voloshin, Prog. Part. Nucl. Phys. **67**, 541 (2012).
[75] S. A. Voloshin [ALICE Collaboration], Nucl. Phys. A **904-905**, 90c (2013).
[76] E.V. Gorbar, V.A. Miransky, I.A. Shovkovy, X. Wang, Phys. Rev. D **88 (2)**, 025025 (2013).
[77] J. C. Dunlop, M. A. Lisa and P. Sorensen, Phys. Rev. C **84**, (2011) 044914.
[78] J. Xu, L. -W. Chen, C. M. Ko and Z. -W. Lin, Phys. Rev. C **85**, (2012) 041901 (2012).
[79] L. Adamczyk *et al.* (STAR Collaboration), Phys. Rev. Lett. **114**, (2015) 252302.
[80] J. Adam *et al.* (ALICE Collaboration), Phys. Rev. C **93**, 044903 (2016).

[81] L. Adamczyk et al. [STAR Collaboration], Phys. Rev. Lett. **110**, 142301 (2013).
[82] J. M. Campbell and M. A. Lisa, Journal of Physics: Conference Series **446**, 012014 (2013).
[83] Y. Burnier, D.E. Kharzeev, J. Liao, H.-U. Yee, arXiv: 1208.2537 (2012).
[84] H. Yee and Y. Yin, Phys. Rev. C **89** (2014) 044909 .
[85] S. A. Voloshin and R. Belmont, Nucl. Phys. A **931**, 992 (2014).
[86] A. Bzdak and P. Bozek, arXiv:1303.1138.
[87] Q.-Y. Shou [STAR Collaboration], Nucl. Phys. A **931**, 758 (2014).
[88] Y. Hatta, A. Monnai and B. W. Xiao, Nucl. Phys. A **947**, 155 (2016).
[89] Q.-Y. Shou [STAR Collaboration], "Charge asymmetry dependence of K v_2 in Au+Au collisions at STAR", Workshop on Chirality, Vorticity and Magnetic Field in Heavy Ion Collisions, 2016; http://starmeetings.physics.ucla.edu/sites/default/files/qiye_shou.pdf
[90] J. Schukraft, A. Timmins and S. A. Voloshin, Phys. Lett. B **719**, 394 (2013).
[91] J. -Y. Ollitrault, A. M. Poskanzer and S. A. Voloshin, Phys. Rev. C **80**, 014904 (2009).
[92] W.-T. Deng, X.-G. Huang, G.-L. Ma, G. Wang, arXiv:1607.04697.
[93] S. Raman, C. W. G. Nestor, Jr and P. Tikkanen, Atom. Data Nucl. Data Tabl. **78**, 1 (2001).
[94] B. Pritychenko, M. Birch, B. Singh and M. Horoi, Atom. Data Nucl. Data Tabl. **107**, 1 (2016).
[95] P. Moller, J. R. Nix, W. D. Myers and W. J. Swiatecki, Atom. Data Nucl. Data Tabl. **59**, 185 (1995).
[96] W. T. Deng and X. G. Huang, Phys. Rev. C **85**, 044907 (2012).
[97] W. T. Deng and X. G. Huang, Phys. Lett. B **742**, 296 (2015).